INVITED PAPER

Using High-Resolution Airborne and Satellite Imagery to Assess Crop Growth and Yield Variability for Precision Agriculture

In this paper, an overview is given on the use of airborne multispectral and hyperspectral imagery and high-resolution satellite imagery for assessing crop growth and yield variability.

By Chenghai Yang, James H. Everitt, Qian Du, *Senior Member IEEE*, Bin Luo, *Member IEEE*, and Jocelyn Chanussot, *Fellow IEEE*

ABSTRACT | With increased use of precision agriculture techniques, information concerning within-field crop yield variability is becoming increasingly important for effective crop management. Despite the commercial availability of yield monitors, many crop harvesters are not equipped with them. Moreover, yield monitor data can only be collected at harvest and used for after-season management. On the other hand, remote sensing imagery obtained during the growing season can be used to generate yield maps for both within-season and after-season management. This paper gives an overview on the use of airborne multispectral and hyperspectral imagery and high-resolution satellite imagery for assessing crop growth and yield variability. The methodologies for image acquisition and processing and for the integration and analysis of image and yield data are discussed. Five application examples are provided to illustrate how airborne multispectral and hyperspectral imagery and high-resolution satellite imagery have been used for mapping crop yield variability. Image processing techniques including vegetation indices, unsupervised classification, correlation and regression analysis, principal component analysis, and supervised and unsupervised linear spectral unmixing are used in these examples. Some of the advantages and limitations on the use of different types of remote sensing imagery and analysis techniques for yield mapping are also discussed.

KEYWORDS | Hyperspectral imagery; image analysis; multispectral imagery; precision agriculture; satellite imagery; yield variability

Manuscript received February 5, 2012; revised April 5, 2012; accepted April 5, 2012. Date of publication July 10, 2012; date of current version February 14, 2013.
C. Yang is with the USDA-ARS Southern Plains Agricultural Research Center, College Station, TX 77845 USA (e-mail: chenghai.yang@ars.usda.gov).
J. H. Everitt is with the USDA-ARS Kika de la Garza Subtropical Agricultural Research Center, Weslaco, TX 78596 USA.
Q. Du is with the Department of Electrical and Computer Engineering, Mississippi State University, Mississippi State, MS 39762 USA.
B. Luo is with the State Key Laboratory of Information Engineering in Surveying, Mapping and Remote Sensing, Wuhan University, Wuhan, Hubei 430079, China.
J. Chanussot is with the Department of Image and Signal, GIPSA-Lab, Grenoble Institute of Technology, Grenoble 38402, France.

Digital Object Identifier: 10.1109/JPROC.2012.2196249

I. INTRODUCTION

Crop yield is perhaps the most important piece of information for crop management in precision agriculture. It integrates the effects of various spatial variables such as soil properties, topography, plant population, fertilization, irrigation, and pest infestations. A yield map can therefore be an indispensable input for site-specific operations either by

itself or in combination with other spatial information [1]. With technological advances in electronic sensors and Global Position Systems (GPSs), harvester-mounted yield monitors have become commercially available for many crops. Farmers and researchers are able to collect intensive and accurate yield data simply and inexpensively during harvest. Yield maps can be generated immediately following data collection to show yield patterns within fields. These maps not only help identify within-field spatial variability for variable rate applications, but also enable farmers and researchers to evaluate the economic returns of different farming management strategies [2], [3]. In addition, yield maps are important for field-level improvements, such as drainage, land leveling, irrigation, fencing, and for off-field information use [4].

Despite the commercial availability and increased use of yield monitors, many harvesters are not equipped with them. Moreover, yield monitor data can only be used for after-season management, whereas some problems such as nutrient deficiencies, water stress, or pest infestations should be managed during the growing season. Therefore, within-season estimates of relative yield variation will be more useful for addressing these problems. Traditional satelite imagery such as Landsat and SPOT has long been used to monitor crop growing conditions and to estimate crop yields over large geographic areas. However, this type of imagery has limited use for assessing within-field yield variability because of its coarse spatial resolution. Therefore, airborne multispectral and hyperspectral imagery and high-resolution satellite imagery such as QuickBird have been used for this purpose. Remote sensing imagery obtained during the growing season has the potential not only for after-season management, but also for within-season management. Additionally, yield maps derived from remote sensing imagery can be used as an alternative when yield monitor data are not available.

The objectives of this paper are to review and illustrate with application examples on the use of airborne multispectral and hyperspectral imagery and high-resolution satellite imagery for mapping crop growth and yield variability for precision agriculture applications.

II. METHODOLOGIES AND EXAMPLES

A. Airborne Multispectral Imagery and Ground Sampling to Generate Yield Maps

Airborne multispectral imaging systems provide image data at fine spatial resolutions and at narrow spectral bands and have the real-time monitoring capability. Airborne multispectral imagery has been related to crop yields based on samples collected on field plots or in various sampling patterns [5]–[10].

Yang and Anderson [7], [11] evaluated airborne multispectral digital video imagery for delineating within-field management zones and for mapping yield variability in grain sorghum. An airborne multispectral imaging system described by Everitt *et al.* [12] was used for image acquisition. The system consists of three charge-coupled device (CCD) analog video cameras, which are equipped with a visible green (555–565 nm) filter, a visible red (625–635 nm) filter, and a near-infrared (NIR, 845–857 nm) filter, respectively. The NIR, red, and green signals from the cameras were digitized and combined to produce color-infrared (CIR) composite images with 640 × 480 pixels and 256 gray levels.

Fig. 1(a) shows a CIR image for a 6-ha grain sorghum field in south Texas in 1995. The image was acquired at an attitude of 1300 m when plants were fully expanded, corresponding to the bloom to soft dough stages of plant growth. The pixel size of the image was 1.4 m. On the CIR image, healthy plants have a reddish–magenta color, while

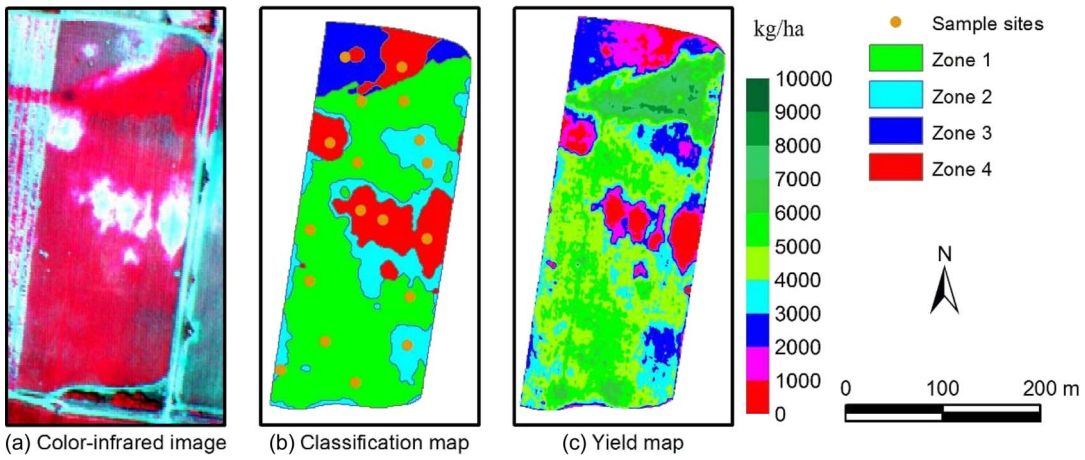

Fig. 1. *(a) A color-infrared digital image, (b) a four-zone classification map, and (c) a yield map generated from the CIR image based on a regression equation relating yield to NDVI for a 6-ha grain sorghum field in south Texas in 1995.*

chlorotic plants and areas with large soil exposure have a whitish and grayish tone. The CIR image was classified into four spectral zones using an unsupervised classification procedure [Fig. 1(b)]. Unsupervised classification is an iterative process of grouping pixels into a finite number of classes or zones of similar spectral characteristics. The advantage of classifying image data into discrete zones is the reduced variance within each zone and therefore the reduced number of ground samples required to identify the cause of the variation within fields. These zones can be used as management zones for plant and soil sampling and for other farming operations. A stratified random sampling approach was used to generate the sampling sites for the field. This approach assured that every zone of the map was sampled, while simultaneously preserving an element of randomness. The sampling sites are also shown in the classification map.

Correlation analysis showed that yield is significantly related to the normalized difference vegetation index (NDVI) with a correlation coefficient of 0.95. The important implication of this strong correlation is that grain yield can be estimated from NDVI for every pixel of the image. Fig. 1(c) shows a grain yield map generated from the digital image based on the regression equation between yield and NDVI for the field. This map clearly shows the spatial variability in yield within the field. Compared with the CIR image and classification map, the yield map has a similar spatial pattern, but reveals more variations within the zones.

This study demonstrates how airborne multispectral imagery can be used in conjunction with ground sampling, GPS, Geographic Information Systems (GISs), and image processing techniques for mapping within-field yield variability. The unsupervised classification technique is effective to separate the imagery into spectral zones with different production levels. Multispectral images are also proven instrumental in modeling the spatial variability of yield. Significant correlations existed between grain yield and image data. These results indicate that images acquired during growing season can be used not only to identify management zones, but also to map the variation in yield within fields.

B. Relationships Between Yield Monitor Data and Multidate Multispectral Imagery

With the increased use of harvester-mounted yield monitors, intensive yield data can be collected from a field. The availability of both yield monitor data and remote sensing imagery allows the relations between yield and spectral image data to be evaluated more robustly and thoroughly than the use of limited numbers of yield samples. Many researchers have evaluated the relationships between yield monitor data and airborne multispectral imagery [13]–[17].

Yang and Everitt [16] evaluated the relationships between yield monitor data and airborne multispectral digital imagery for grain sorghum. An airborne three-camera imaging system described by Escobar *et al.* [18] was used. This system consists of three true digital CCD cameras that are filtered to the same green, red, and NIR wavebands as those in the previous imaging system to provide 8-b images with 1024×1024 pixel resolution. Images with pixel sizes of 0.85–0.92 m were acquired from multiple grain sorghum fields on five different dates: April 16 and 22, May 18 and 29, and June 16, 1998. Yield monitor data with a spatial resolution of 8.7 m were collected using a Yield Monitor 2000 system (Ag Leader Technology, Ames, IA) from the field on June 29, 1998.

Fig. 2(a) and (b) shows two of the five CIR digital images obtained from a 21-ha field. These images clearly reveal distinct details of the spatial plant growth variation within the field over the growing season. Table 1 summarizes correlation coefficients of yield with the three bands and the four vegetation indices based on the yield monitor data and the images obtained from the grain sorghum field on the five dates. Grain yield was significantly related to each of the three bands and each of the four vegetation indices for all the five dates. The general progression of the correlations over the growing season can be clearly seen from Table 1. The correlations consistently increased from April 15 to May 18 until the crop reached peak vegetative development. For the last two dates, the correlations tended to level off, even though they fluctuated somewhat for all the spectral variables.

Regression analysis showed R^2-values for the best fitting stepwise regression models relating grain yield to the NIR, red, and green bands were 0.61, 0.65, 0.76, 0.79, and 0.74, respectively, for the five dates. The May 29 image gave the highest correlation and accounted for 79% of the variability in yield, though the May 18 and June 16 images were almost equally good. Therefore, images taken around or shortly after peak vegetative development could be a better yield indicator than those taken on early or late stages for grain sorghum. Fig. 2(c) and (d) shows the yield maps generated from yield monitor data and from the May 29 image, respectively. Overall pattern in the yield map from the image is very similar to that in the map from the yield monitor data. In contrast, the image-derived yield map gives more details because the image data had a finer spatial resolution than the yield monitor data (8.7 m). Moreover, the spatial patterns displayed on both yield maps are similar to those on the CIR images, indicating yield patterns can be observed from airborne multispectral imagery taken during the growing season.

It should be noted that the regression equations relating yield to the spectral bands or vegetation indices are field specific or location specific and may not hold valid for other fields in the same season or for the same fields or location in the following season because many other factors can affect plant growth and yield. Currently, yield monitors are available for many crops, but only a small percentage of the farmers are using them. Airborne

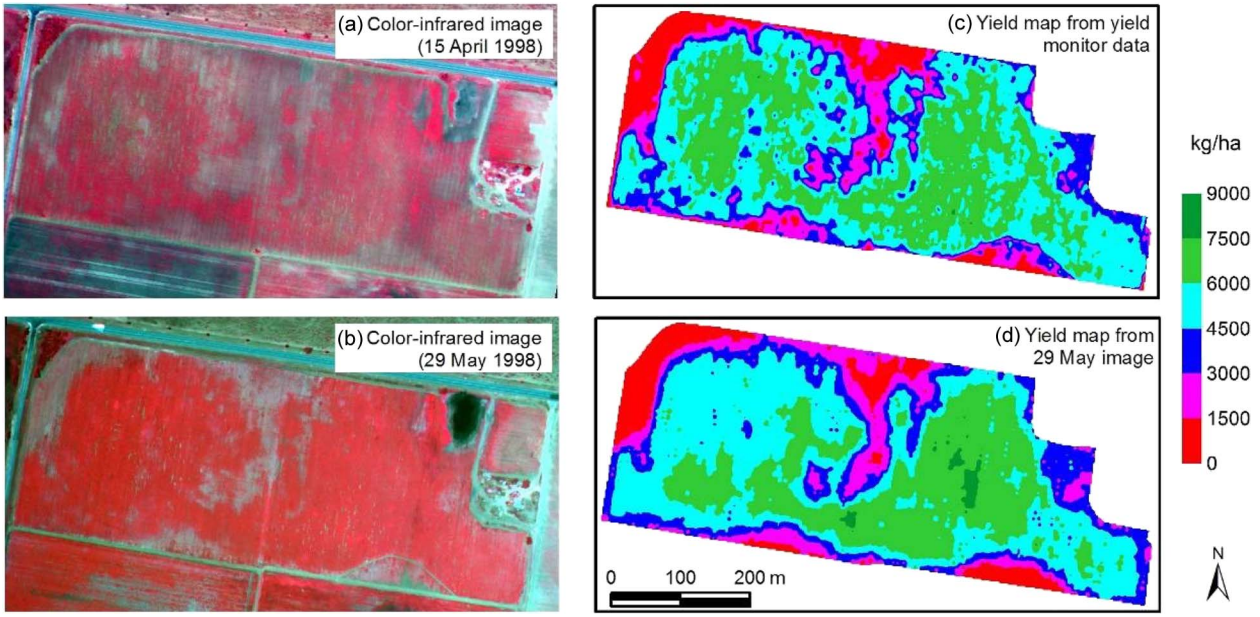

Fig. 2. *(a) A color-infrared image acquired in the early growing season, (b) a color-infrared image acquired after peak vegetative growth, (c) a yield map generated from yield monitor data, and (d) a yield map derived from the May 29 image based on a regression equation relating yield to the three bands in the image for a 21-ha grain sorghum field in south Texas in 1998.*

imagery in conjunction with ground sampling and regression analysis provides an alternative for yield mapping for fields where yield monitor data are not available. Imagery acquired on different dates in this study provided some clue as to the optimal time period for image acquisition for yield estimation. While accurate estimates of yield are not always possible in the middle of the season, yield patterns and within-field management zones identified from airborne multispectral imagery can be very useful for both within-season and after-season management.

C. Airborne Hyperspectral Imagery and Yield Monitor Data for Mapping Yield Variability

Hyperspectral imagery contains tens to hundreds of narrowbands and provides additional information that multispectral data may have missed. These almost

Table 1 Correlation Coefficients (r) of Yield With Three Bands and Four Vegetation Indices Based on Yield Monitor Data and Color-Infrared Images Obtained From a Grain Sorghum Field on Five Dates in South Texas in 1998

Spectral variable	Imaging date				
	April 15	April 22	May 18	May 29	June 16
NIR[a]	0.60[b]	0.66	0.79	0.74	0.84
Red	-0.50	-0.57	-0.75	-0.70	-0.76
Green	-0.38	-0.41	-0.81	-0.59	-0.62
NR	0.69	0.65	0.81	0.76	0.83
NG	0.75	0.79	0.87	0.84	0.85
NDVI	0.72	0.75	0.80	0.83	0.85
GNDVI	0.77	0.81	0.85	0.86	0.86

[a] NIR = near-infrared, NR = NIR/Red, NG = NIR/Green, NDVI = (NIR - Red)/(NIR + Red), GNDVI = (NIR - Green)/(NIR + Green).
[b] All r-values are significant at the 0.0001 level.

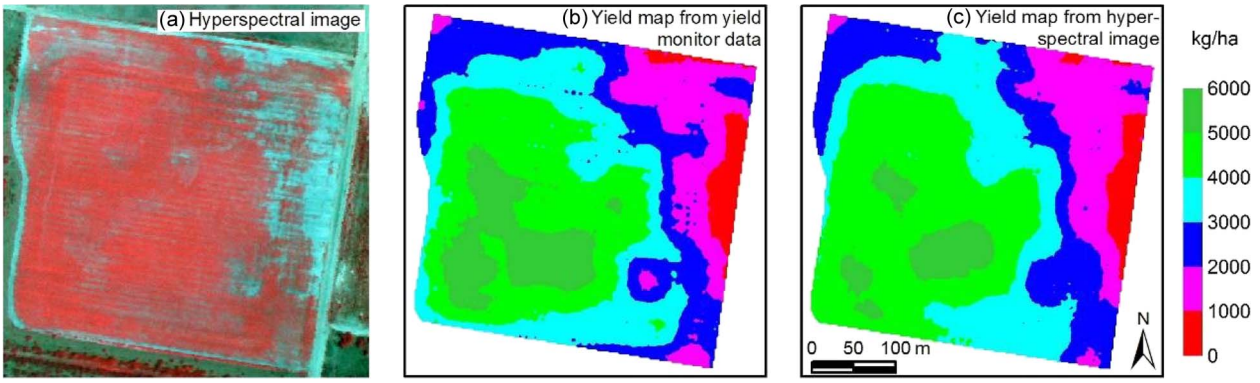

Fig. 3. *(a) A color-infrared composite extracted from a 102-band hyperspectral image, (b) a yield map generated from yield monitor data, and (c) a yield map derived from the hyperspectral image based on a regression equation relating yield to seven significant bands in the image for a 14-ha grain sorghum field in south Texas in 2000.*

continuous spectral data have the potential for better differentiation and estimation of biophysical attributes for some applications. Airborne hyperspectral imagery has been evaluated for estimating crop yields [19]–[23].

Yang *et al.* [20] examined the correlations between yield monitor data and airborne hyperspectral imagery for grain sorghum. An airborne hyperspectral imaging system described by Yang *et al.* [24] was used for image acquisition. The system consists of a digital CCD camera, a prism–grating–prism imaging spectrograph, and a personal computer (PC) equipped with a frame grabbing board and camera utility software. The system is configured to capture 12-b images with a swath of 640 pixels and 128 bands from 457.2 to 921.7 nm at 3.63-nm intervals. The first five bands and the last 21 bands were removed from each image and the remaining 102 bands with wavelengths from 475 to 845 nm were used for analysis. Yield monitor data were collected using the same Ag Leader yield monitor 2000 system.

Fig. 3(a) shows a CIR composite extracted from the 102-band hyperspectral image for a 14-ha grain sorghum field in south Texas. The hyperspectral image was taken around the peak plant development for the crop on April 27, 2000. Poor plant canopies in the problem areas were mainly due to the very sandy soil. Plants in those areas had poor stand and low canopy cover because of the low water and nutrient holding capability of the sandy soil.

Grain yield was significantly negatively related to the visible bands and positively related to the NIR bands. Correlation coefficients among the 102 bands varied from −0.80 to 0.84. To eliminate the redundancy in the image data, the original 102-band image was transformed into a set of unrelated, independent principal components [25]. Stepwise regression results for relating grain yield to the first ten principal components show that five of the ten principal components were found to be significant and explained 80% of the variability in yield. To identify the bands or combinations of bands that were particularly responsive to yield variability, stepwise regression was performed directly on the yield data and the 102-band hyperspectral image data. Seven of the 102 bands were identified to be significant in the final regression equation and explained about 82% of the variability in yield. Fig. 3(b) and (c) show the yield maps generated from yield monitor data and from the seven significant bands in the image, respectively. Although multiple regression can be used to identify the optimum bands for estimating yield, these bands are only the best for the image and yield data from which they are derived and might not be the best for different data sets. For example, Yang *et al.* [21] identified four significant bands, which were completely different from the seven significant bands, to estimate yield for another grain sorghum field.

The *r*-values for the six possible NDVI-type indices (NIR versus blue, NIR versus green, NIR versus red, red versus blue, red versus green, and green versus blue) derived from the four simulated Landsat ETM+ broad bands ranged from 0.60 for the red and blue pair to 0.83 for the NIR and red pair. Based on stepwise regression analysis, the four broad bands accounted for 76% of the variability in yield, compared with 82% of the variability explained by the seven significant narrowbands. Therefore, the hyperspectral image provided better yield estimation than the simulated broad band multispectral image. Fig. 3(b) and (c) presents the yield maps generated from yield monitor data and from the hyperspectral image with the regression equation relating yield to the seven significant bands. The spatial patterns displayed on both yield maps are similar, indicating yield patterns can be estimated from airborne hyperspectral imagery taken during the growing season.

Fig. 4 shows a contour map of absolute *r*-values between yield and each of the 5151 (102!/100!/2!) possible NDVI-type indices for the sorghum field. The absolute *r*-values vary from 0 to 0.88 for sorghum. The *r*-values are generally larger when one band has wavelengths smaller than 730 nm and the other band has wavelengths larger

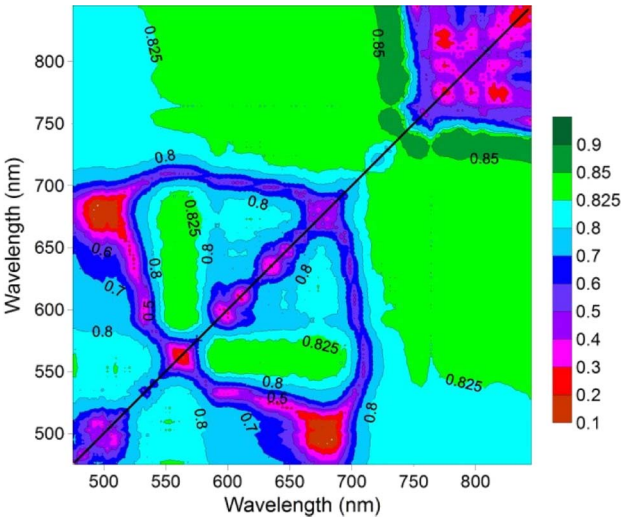

Fig. 4. *A contour map showing absolute correlation coefficients between crop yield and all possible narrowband NDVIs derived from a 102-band airborne hyperspectral image for a 14-ha grain sorghum field in south Texas in 2000. When band i = band j, $NDVI_{ij} = 0$ and correlations do not exist (shown by the diagonal line).*

than 730 nm. However, the best r-values (> 0.85) occur when one band is around 730 nm and the other was over 760 nm for the field. Also large r-values (> 0.825) occur when one band in a pair has wavelengths between 550 and 575 nm and the other has wavelengths between 575 and 690 nm. Based on the contour map of r-values, better NDVI images are more likely to be obtained by selecting one band in the visible region and the other in the NIR region.

D. Applying Linear Spectral Unmixing to Airborne Hyperspectral Imagery for Mapping Yield Variability

Although all possible narrowband NDVIs can be calculated to identify the best NDVI, it is not always practical to do so because of the large number of bands. Moreover, the optimum narrowband NDVI identified for one data set might not be the best for another. Therefore, it is necessary to use a technique that can take advantage of the spectral information in all the bands without the need to choose which bands to use.

Spectral unmixing techniques can be used to quantify crop canopy cover within each pixel of an image and have the potential for mapping the variation in crop yield. Each image pixel contains a spectrum of reflectance values for all the wavebands. These spectra can be regarded as the signatures of ground components such as crop plants or soil, provided that a component, referred to as an endmember, occupies the whole pixel. Spectra from mixed pixels can be analyzed with linear spectral unmixing, which models each spectrum in a pixel as a linear combination of a finite number of spectrally pure spectra of the endmembers in the image, weighted by their fractional abundances [26], [27].

When linear spectral unmixing is applied to an image, it produces a suite of abundance fraction images, one for each endmember in the model. Each fraction image shows the spatial distribution of the spectrally defined component as an NDVI image does. The fractional abundance of crop plants determined from linear spectral unmixing is a more direct measure of plant cover than an NDVI value. Yang *et al.* [23] applied this technique to hyperspectral imagery for mapping the variation in yield in two grain sorghum fields and their results indicate that plant abundance fraction images can be used as relative yield maps. They also examined how variations in endmember spectra affect the results and found that correlation coefficients between yield and unconstrained plant abundance fractions are not sensitive to the selection of plant and soil endmembers, though the correlation coefficients between yield and constrained plant abundance fractions are affected by the choice of endmember spectra.

Linear spectral unmixing analysis requires the spectra of the endmembers. They can be obtained directly from the image, measured on the ground or derived from a spectral library. In this study, crop plants and bare soil were selected as the relevant endmembers. Thus, a simple linear spectral unmixing model has the following form:

$$y_i = a_{i1}x_1 + a_{i2}x_2 + \varepsilon_i, \qquad i = 1, 2, \ldots, n$$

where y_i is the measured reflectance in band i for a pixel; a_{i1} and a_{i2} are the known or measured reflectance in band i for plants and soil, respectively; x_1 and x_2 are the unknown cover fractions or abundances for plants and soil, respectively; ε_i is the residual between measured and modeled reflectance for band i; and n is the number of spectral bands. This model is referred to as the unconstrained linear spectral unmixing model. For the constrained model, the fractional abundances are subject to the nonnegativity constraint and the sum-to-one constraint.

A pair of plant and soil spectra was extracted from the hyperspectral image for the 14-ha grain sorghum field to represent pure and healthy plants and bare soil, respectively, and was used as endmember spectra for spectral unmixing analysis [28]. Each endmember spectrum was the average of about 100 pixels identified for the endmember. Both unconstrained and constrained linear spectral unmixing models were applied to the image, and four fractional images (two unconstrained and two constrained) were generated for the 14-ha sorghum field.

Ideally, abundance values should be within the 0–1 range, but in unconstrained fraction images they can be negative or exceed 1. For example, the unconstrained plant abundance varied from -0.15 to 1.01 and the unconstrained soil abundance varied from 0.02 to 1.16 for the field. This is because spectral unmixing results can be affected by the purity of the endmembers and the number

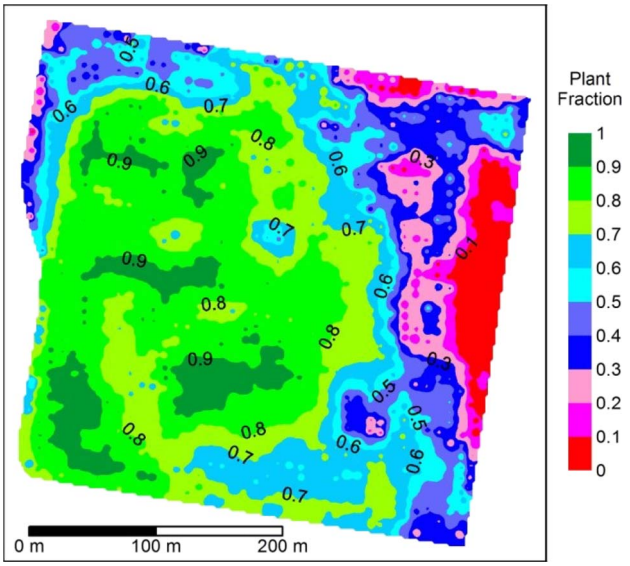

Fig. 5. ***A constrained plant abundance fraction image derived from the 102-band airborne hyperspectral image for a sorghum field in South Texas in 2000 based on a pair of plant and soil endmember spectra extracted from the image.***

of endmembers. The linearity assumption of linear spectral unmixing is at best an approximation of the generally nonlinear mixing of surface components. As expected, the fully constrained fractions had values in the range of 0–1. Fig. 5 shows the fully constrained plant abundance fraction image derived from the hyperspectral image. Red areas have small plant abundance values and represent pixels with a large exposure of soil and sparse plant cover. Conversely, green areas indicate large plant abundance values and represent pixels with dense plant cover.

Mean unconstrained plant and soil abundance fractions were 0.63 and 0.32, indicating mean plant canopy cover was approximately 63% at the time of the image acquisition. The sum of the plant and soil abundance fraction was 0.95. Although the unconstrained model does not force the endmember abundance fractions to sum to 1, the sum is still close to 1, indicating the unconstrained two-endmember linear unmixing model is appropriate for characterizing plant and soil cover in the images. Mean constrained plant and soil abundance fractions were 0.64 and 0.36, respectively, with an expected unity sum.

Correlation analysis showed that yield was positively related to unconstrained and constrained plant abundance fractions, and negatively related to the unconstrained and constrained soil abundance fractions. Unconstrained plant abundance fractions had slightly stronger correlations with yield than the unconstrained soil abundance fractions, whereas constrained plant and soil abundance fractions had identical absolute correlations because they sum to unity. The correlation coefficients with yield were 0.85 for the unconstrained plant abundance fraction and −0.82 for the unconstrained soil abundance fraction. The absolute r-values for both constrained plant and soil abundance fractions were 0.85.

The best NDVIs had larger correlations with yield (0.88) than the best abundance fraction image (0.85). Nevertheless, the best abundance fraction-based r-value (0.85) was better than 97.1% of the 5151 NDVI-based r-values for the sorghum field. Although an NDVI image could provide better r-values than a plant fraction image as shown in this study, the best NDVI identified from one image is unlikely to be the best NDVI for another. Moreover, the best NDVI can only be identified if the yield is known and all possible narrowband NDVIs or at least the NDVIs with red and NIR band pairs are calculated. On the other hand, the plant fraction image can be generated using all the bands and a pair of plant and soil endmember spectra without the need to know the actual yield. It also has the potential to be as good as or even better than the best NDVI. Therefore, linear spectral unmixing techniques can be used alone or in conjunction with other traditional vegetation indices for mapping yield variability.

Traditional supervised unmixing methods, as described above, require reference spectra to be obtained either by measurements in the field or manual selection from the image. Unsupervised spectral unmixing can automatically extract the endmember spectra from the image and therefore is more efficient. There are two approaches to unsupervised spectral unmixing: statistical and geometrical methods [29]. The statistical methods, such as the independent component analysis (ICA) [30] and Bayesian positive source separation (BPSS) [31], extract the endmembers by optimizing some statistical criteria. The geometrical methods are based on the geometrical properties of linear mixture model of hyperspectral data and are generally more adaptive to the data and more efficient. They can be divided into two classes: direct methods (i.e., N-Finder [32], vertex component analysis (VCA) [33], and sequential maximum angle convex cone (SMACC) [34]) and advanced methods (i.e., minimum volume constrained nonnegative matrix factorization (MVCNMF) [35], simplex identification via split augmented Lagrangian (SISAL) [36], and minimum volume simplex analysis (MVSA) [37]). The direct methods extract the extremal points within the data set as endmembers, while the advanced methods attempt either to find the simplex with minimum volume which contains all data points and extract the extremal points of the simplex as endmembers (i.e., SISAL and MVSA) or to minimize the projection error of the data to a subset and use the simplex volume as a regularization term (i.e., MVCNMFT).

Luo *et al.* [38] evaluated two unsupervised linear spectral unmixing approaches, VCA and N-Finder, for estimating crop yield from hyperspectral imagery. The selection for the two direct methods was based on the fact that the hyperspectral imagery had high spatial resolution so that the pure pixel assumption could be satisfied. Moreover,

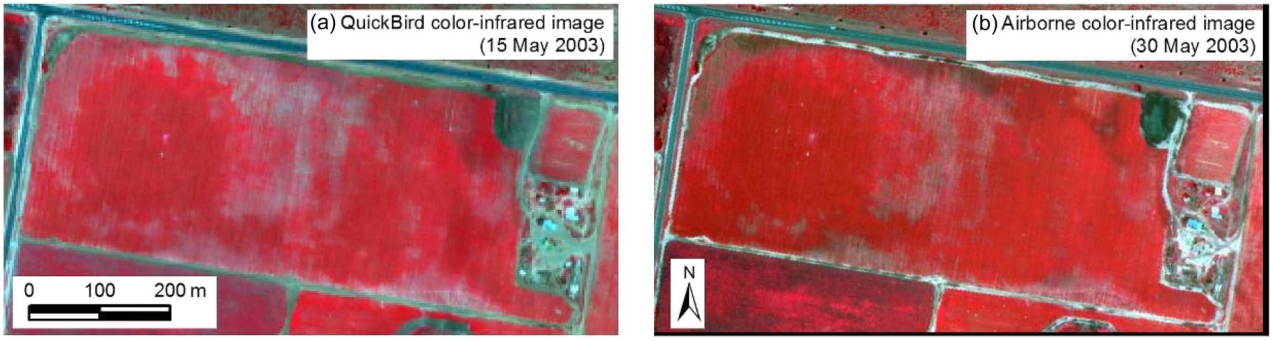

Fig. 6. *(a) A QuickBird color-infrared image and (b) an airborne color-infrared image for a 23-ha grain sorghum field in south Texas in 2003.*

direct methods are generally more efficient than advanced methods. Their results showed that both approaches are as good as the supervised linear unmixing methods (unconstrained and constrained linear spectral unmixing). With unsupervised unmixing, vegetation abundance images can be obtained without the need to manually select endmember spectra. In addition, Luo *et al.* [38] applied the unsupervised approaches on the hyperspectral images taken on two different dates. The results showed that the combination of the vegetation abundances extracted from two dates can improve the correlations with yield.

E. Comparison of QuickBird Satellite Imagery and Airborne Imagery for Mapping Grain Sorghum Yield Patterns

The commercial availability of high-resolution satellite sensors, including IKONOS, QuickBird, SPOT 5, and the more recent GeoEye-1 and WorldView 2 sensors, has opened up new opportunities for mapping within-field variability. These satellite sensors have significantly narrowed the gap in spatial resolution between satellite and airborne imagery. IKONOS and QuickBird imagery has been evaluated for assessing crop yields [17], [39]–[41].

Yang *et al.* [40], [41] compared QuickBird satellite imagery with airborne multispectral imagery for mapping plant growth and yield patterns within grain sorghum and cotton fields. A QuickBird 2.8-m image covering a cropping area in south Texas was acquired in the 2003 growing season. The imagery contained four spectral bands: blue (450–520 nm), green (520–600 nm), red (630–690 nm), and NIR (760–900 nm). The spatial resolution of the image was 2.8 m and the radiometric resolution was 11 b. Airborne CIR imagery was collected using the same imaging system described by Escobar *et al.* [18], except that the acquisition computer and image grabbing cards were upgraded to enhance acquisition speed and to obtain images with 1280 × 1024 pixels. Yield data were collected using a PF3000 yield monitor (Ag Leader Technology).

Fig. 6 shows the CIR composite of the QuickBird image and the airborne CIR image for a 23-ha field in south Texas. The pixel size for the airborne image was 0.92 m, compared to the 2.8 m for the satellite image. Both the QuickBird and MegaPlus images reveal distinct plant growth patterns within the two fields. The QuickBird image was taken at the bloom stage of the plant development (May 15), shortly after the peak growth for the crop. The airborne image was taken 15 days later when the plants were primarily at the soft-dough stage. Despite the difference in plant growth stages, the plants had similar canopy cover during the imaging period. Although the pixel sizes are different (2.8 versus 0.92 m), both types of images look fairly similar.

Correlation analysis results between yield and vegetation indices (band ratios and NDVI-type indices) at different pixel sizes showed that the NIR/green ratio provided best *r*-values for both types of imagery and *r*-values tended to increase with pixel size. For the airborne imagery, the best *r*-value was 0.78 at the original pixel size, 0.81 at 2.8 m (QuickBird pixel size), and 0.85 at 8.4 m (close to harvest swath). For the QuickBird image, the best *r*-value was 0.83 at 2.8 m and 0.88 at 8.4 m.

Based on stepwise regression analysis at the 8.4-m resolution, the airborne image explained 77% of the variability in yield, while the QuickBird image explained 80% of the variability with the green, red, and NIR bands and 81% of the variability with all four bands. Although the QuickBird imagery had slightly higher R^2 values than the airborne imagery, both types of imagery accounted for essentially the same amount of yield variability, indicating that the QuickBird imagery is as effective as the airborne imagery for yield estimation.

III. CONCLUSION

The review and application examples presented in this paper demonstrate that airborne multispectral and hyperspectral imagery and high-resolution satellite imagery can be useful data sources for estimating and mapping within-field crop yield variability for precision agriculture. High-resolution airborne and satellite imagery taken during the growing season can be used to monitor crop growing

conditions and identify potential problems that could be addressed within the growing season. The imagery taken around peak vegetative development can also be used to generate yield maps to document the spatial variation in yield. Although airborne multispectral imagery is sufficient for these purposes, airborne hyperspectral imagery has the potential to provide additional information that multispectral data may have missed. Linear spectral unmixing techniques can be used alone or in conjunction with traditional vegetation indices for estimating crop fractional cover and mapping yield variability. High-resolution QuickBird imagery can be as effective as airborne multispectral imagery for mapping yield variability. As more airborne and high-resolution satellite imagery is becoming available, more research is needed to compare different types of imagery and data analysis techniques for yield estimation and other precision agriculture applications under various crop environments. ■

Acknowledgment

The authors would like to thank R. Davis, D. Escobar, and F. Gomez of USDA-ARS, Weslaco, TX, for acquiring the airborne imagery; W. Swanson and J. Forward of USDA-ARS, Weslaco, TX, for ground data collection and image rectification; and D. Murden, M. Willis, and B. Campbell of Rio Farms, Inc., Monte Alto, TX, for allowing them to use their fields and harvest equipment.

REFERENCES

[1] S. W. Searcy, J. K. Schueller, Y. H. Bae, S. C. Borgelt, and B. A. Stout, "Mapping of spatially variable yield during grain combining," *Trans. ASAE*, vol. 32, pp. 826–829, 1989.

[2] S. J. Birrell, K. A. Sudduth, and S. C. Borgelt, "Comparison of sensors and techniques for crop yield mapping," *Comput. Electron. Agriculture*, vol. 14, pp. 215–233, 1996.

[3] C. Yang, J. H. Everitt, and J. M. Bradford, "Comparisons of uniform and variable rate nitrogen and phosphorus fertilizer applications for grain sorghum," *Trans. ASAE*, vol. 44, no. 2, pp. 201–209, 2001.

[4] S. M. Swinton and J. Lowenberg-DeBoer, "Evaluating the profitability of site-specific farming," *J. Production Agriculture*, vol. 11, no. 4, pp. 439–446, 1998.

[5] A. J. Richardson, M. D. Heilman, and D. E. Escobar, "Estimating grain sorghum yield from video and reflectance based PVI measurements at peak canopy development," *J. Imag. Technol.*, vol. 16, no. 3, pp. 104–109, 1990.

[6] C. L. Wiegand, J. D. Rhoades, D. E. Escobar, and J. H. Everitt, "Photographic and videographic observations for determining and mapping the response of cotton to soil salinity," *Remote Sens. Environ.*, vol. 49, pp. 212–223, 1994.

[7] C. Yang and G. L. Anderson, "Airborne videography to identify spatial plant growth variability for grain sorghum," *Precision Agriculture*, vol. 1, no. 1, pp. 67–79, 1999.

[8] J. F. Shanahan, J. S. Schepers, D. D. Francis, G. E. Varvel, W. W. Wilhelm, J. M. Tringe, M. R. Schlemmer, and D. J. Major, "Use of remote sensing imagery to estimate corn grain yield," *Agronomy J.*, vol. 93, pp. 583–589, 2001.

[9] C. T. Leon, D. R. Shaw, M. S. Cox, M. J. Abshire, B. Ward, M. C. Wardlaw, and C. Watson, "Utility of remote sensing in predicting crop and soil characteristics," *Precision Agriculture*, vol. 4, no. 4, pp. 359–384, 2003.

[10] D. Inman, R. Khosla, R. Reich, and D. G. Westfall, "Normalized difference vegetation index and soil color-based management zones in irrigated maize," *Agronomy J.*, vol. 100, pp. 60–66, 2008.

[11] C. Yang and G. L. Anderson, "Mapping grain sorghum yield variability using airborne digital videography," *Precision Agriculture*, vol. 2, no. 1, pp. 7–23, 2000.

[12] J. H. Everitt, D. E. Escobar, I. Cavazos, J. R. Noriega, and M. R. Davis, "A three-camera multispectral digital video imaging system," *Remote Sens. Environ.*, vol. 54, pp. 333–337, 1995.

[13] G. B. Senay, A. D. Ward, J. G. Lyon, N. R. Fausey, and S. E. Nokes, "Manipulation of high spatial resolution aircraft remote sensing data for use in site-specific farming," *Trans. ASAE*, vol. 41, no. 2, pp. 489–495, 1998.

[14] S. GopalaPillai and L. Tian, "In-field variability detection and spatial yield modeling for corn using digital aerial imaging," *Trans. ASAE*, vol. 42, no. 6, pp. 1911–1920, 1999.

[15] C. Yang, J. H. Everitt, J. M. Bradford, and D. E. Escobar, "Mapping grain sorghum growth and yield variations using airborne multispectral digital imagery," *Trans. ASAE*, vol. 43, no. 6, pp. 1927–1938, 2000.

[16] C. Yang and J. H. Everitt, "Relationships between yield monitor data and airborne multidate multispectral digital imagery for grain sorghum," *Precision Agriculture*, vol. 3, no. 4, pp. 373–388, 2002.

[17] A. Dobermann and J. L. Ping, "Geostatistical integration of yield monitor data and remote sensing improves yield maps," *Agronomy J.*, vol. 96, pp. 285–297, 2004.

[18] D. E. Escobar, J. H. Everitt, J. R. Noriega, M. R. Davis, and I. Cavazos, American Society for Photogrammetry and Remote Sensing, "A true digital imaging system for remote sensing applications," in *Proc. 16th Biennial Workshop Color Photography Videography Resource Assessment*, Bethesda, MD, 1997, pp. 470–484.

[19] P. K. Goel, S. O. Prasher, J. A. Landry, R. M. Patel, A. A. Viau, and J. R. Miller, "Estimation of crop biophysical parameters through airborne and field hyperspectral remote sensing," *Trans. ASAE*, vol. 46, no. 4, pp. 1235–1246, 2003.

[20] C. Yang, J. H. Everitt, and J. M. Bradford, "Airborne hyperspectral imagery and yield monitor data for estimating grain sorghum yield variability," *Trans. ASAE*, vol. 47, no. 3, pp. 915–924, 2004.

[21] C. Yang, J. H. Everitt, J. M. Bradford, and D. Murden, "Airborne hyperspectral imagery and yield monitor data for mapping cotton yield variability," *Precision Agriculture*, vol. 5, no. 5, pp. 445–461, 2004.

[22] P. J. Zarco-Tejada, S. L. Ustin, and M. L. Whiting, "Temporal and spatial relationships between within-field yield variability in cotton and high-spatial hyperspectral remote sensing imagery," *Agronomy J.*, vol. 97, pp. 641–653, 2005.

[23] C. Yang, J. H. Everitt, and J. M. Bradford, "Airborne hyperspectral imagery and linear spectral unmixing for mapping variation in crop yield," *Precision Agriculture*, vol. 8, no. 6, pp. 279–296, 2007.

[24] C. Yang, J. H. Everitt, M. R. Davis, and C. Mao, "A CCD camera-based hyperspectral imaging system for stationary and airborne applications," *Geocarto Int. J.*, vol. 18, no. 2, pp. 71–80, 2003.

[25] M. J. Canty, *Image Analysis, Classification, and Change Detection in Remote Sensing With Algorithms for ENVI/IDL*, 2nd ed. New York: Taylor & Francis, 2010, pp. 89–91.

[26] J. B. Adams, M. O. Smith, and P. E. Johnson, "Spectral mixture modeling: A new analysis of rock and soil types at the Viking Lander 1 site," *J. Geophys. Res.*, vol. 91, pp. 8098–8112, 1986.

[27] M. O. Smith, S. L. Ustin, J. B. Adams, and A. R. Gillespie, "Vegetation in deserts: I. A regional measure of abundance from multispectral images," *Remote Sens. Environ.*, vol. 31, pp. 1–26, 1990.

[28] C. Yang, J. H. Everitt, and Q. Du, "Applying linear spectral unmixing to airborne hyperspectral imagery for mapping yield variability in grain sorghum and cotton fields," *J. Appl. Remote Sens.*, vol. 4, 041887, 2010.

[29] M. Parente and A. Plaza, "Survey of geometric and statistical unmixing algorithms for hyperspectral images," in *Proc. IEEE GRSS Workshop Hyperspectral Image Signal Process., Evol Remote Sens.*, Reykjavik, Iceland, 2010, DOI: 10.1109/WHISPERS.2010.5594929.

[30] J. Nascimento and J. B. Dias, "Does independent component analysis play a role in unmixing hyperspectral data," *IEEE Trans. Geosci. Remote Sens.*, vol. 43, no. 1, pp. 175–187, Jan. 2005.

[31] S. Moussaoui, H. Hauksdottir, F. Schmidt, C. Jutten, J. Chanussot, D. Brie, S. Doute, and J. Benediktsson, "On the decomposition of mars hyperspectral data by ICA and Bayesian positive source separation," *Neurocomputing*, vol. 71, pp. 2194–2208, 2008.

[32] M. E. Winter, "Fast autonomous spectral end-member determination," in *Proc. 13th Int. Conf. Appl. Geologic*, Vancouver, BC, Canada, 1999, vol. 2, pp. 337–344.

[33] J. Nascimento and J. B. Dias, "Vertex component analysis: A fast algorithm to unmix hyperspectral data," *IEEE Trans. Geosci. Remote Sens.*, vol. 43, no. 4, pp. 898–910, Apr. 2005.

[34] J. Gruninger, A. J. Ratkowski, M. L. Hoke, S. S. Shen, and P. E. Lewis, "The sequential maximum angle convex cone (SMACC) endmember model," *Proc. SPIE—Algorithms and Technologies for Multispectral, Hyperspectral, and Ultraspectral Imagery X*, vol. 5425, no. 1, pp. 1–14, 2004.

[35] L. Miao and H. Qi, "Endmember extraction from highly mixed data using minimum volume constrained nonnegative matrix factorization," *IEEE Trans. Geosci. Remote Sens.*, vol. 45, no. 3, pp. 765–777, Mar. 2007.

[36] J. Bioucas-Dias, "A variable splitting augmented Lagrangian approach to linear spectral unmixing," in *Proc. 1st IEEE GRSS Workshop Hyperspectral Image Signal Process.*, Grenoble, France, 2009, DOI: 10.1109/WHISPERS.2009.5289072.

[37] J. Li and J. M. Bioucas-Dias, "Minimum volume simplex analysis: A fast algorithm to unmix hyperspectral data," in *Proc. IEEE Int. Geosci. Remote Sens. Symp.*, Boston, MA, 2008, vol. 3, pp. 250–253.

[38] B. Luo, C. Yang, and J. Chanussot, "Linear unmixing of multidate hyperspectral imagery for crop yield estimation," in *Proc. IEEE Int. Geosci. Remote Sens. Symp.*, 2011, pp. 1573–1576.

[39] J. Chang, D. E. Clay, K. Dalsted, S. Clay, and M. O'Neill, "Corn (*Zea mays* L.) yield prediction using multispectral and multidate reflectance," *Agronomy J.*, vol. 95, pp. 1447–1453, 2003.

[40] C. Yang, J. H. Everitt, and J. M. Bradford, "Comparison of QuickBird satellite imagery and airborne imagery for mapping grain sorghum yield patterns," *Precision Agriculture*, vol. 7, no. 1, pp. 33–44, 2006.

[41] C. Yang, J. H. Everitt, and J. M. Bradford, "Evaluating high resolution QuickBird satellite imagery for estimating cotton yield," *Trans. ASAE*, vol. 49, no. 5, pp. 1599–1606, 2006.

ABOUT THE AUTHORS

Chenghai Yang received the B.S. and M.S. degrees in agricultural engineering from Northwest A&F University, Yangling, Shaanxi, China, in 1983 and 1986, respectively and the Ph.D. degree in agricultural engineering from the University of Idaho, Moscow, in 1994.

He was an Agricultural Engineer with the USDA-Agricultural Research Service's Kika De La Garza Agricultural Research Center, Weslaco, TX, from 1995 to 2012. Since 2012, he has been with the USDA-ARS Southern Plains Agricultural Research Center, College Station, TX. His research has been focused on the use of remote sensing and other spatial information technologies for precision agriculture and pest management. He has authored/coauthored over 250 journal articles and other technical publications.

Dr. Yang is a member of four professional societies, including the American Society for Photogrammetry and Remote Sensing (ASPRS), and holds various committee assignments. He serves as an Editor or an Associate Editor for five technical journals, as a reviewer for over 30 technical journals, and as a technical expert or panelist for several international research programs. He cochaired or served as academic committee chair/member for several international conferences. He is recognized nationally and internationally for his research on airborne multispectral and hyperspectral remote sensing for agricultural applications. He has been invited to give numerous presentations at international conferences in many countries, and is regularly sought out for technical consultation by colleagues from many countries in the areas of precision agriculture and remote sensing.

James H. Everitt received the B.S. degree in wildlife science from Texas A&M University, College Station, in 1969 and the M.S. degree in range science from Texas A&M University, Kingsville, in 1972.

From 1972 to his retirement in 2010, he was a Range Scientist with the USDA-Agricultural Research Service's Kika De La Garza Agricultural Research Center, Weslaco, TX. Since then, he has been a collaborator with the USDA Weslaco Research Center. During his career, he has conducted remote sensing research for agricultural applications and natural resource management. He has authored/coauthored over 300 scientific publications.

Qian Du (Senior Member, IEEE) received the Ph.D. degree in electrical engineering from the University of Maryland Baltimore County, Baltimore, in 2000.

She was with the Department of Electrical Engineering and Computer Science, Texas A&M University, Kingsville, from 2000 to 2004. She joined the Department of Electrical and Computer Engineering, Mississippi State University, Mississippi State, in fall 2004, where she is currently an Associate Professor. Her research interests include hyperspectral remote sensing image analysis, pattern classification, data compression, and neural networks.

Dr. Du currently serves as Co-Chair for the Data Fusion Technical Committee of the IEEE Geoscience and Remote Sensing Society (GRSS). She also serves as an Associate Editor for the IEEE Journal of Selected Topics in Applied Earth Observations and Remote Sensing and the IEEE Signal Processing Letters. She received the 2010 Best Reviewer award from IEEE GRSS for her service to the IEEE Geoscience and Remote Sensing Letters. She is the General Chair for the 4th IEEE GRSS Workshop on Hyperspectral Image and Signal Processing: Evolution in Remote Sensing (WHISPERS). She is a member of the International Society for Optics and Photonics (SPIE), the American Society of Photogrammetry and Remote Sensing (ASPRS), and the American Society for Engineering Education (ASEE).

Bin Luo (Member, IEEE) received the M.Sc. degree in image processing from the Ecole Normale Supérieure de Cachan (ENS Cachan), Cachan, France, in 2004 and the Ph.D. degree in image and signal processing from the École Nationale Supérieure des Télécommunications (ENST), Paris, France, in 2007.

He worked as a Postdoctoral Researcher in the Grenoble Images Speech Signals and Automatics Laboratory (GIPSA-Lab), Grenoble, France, from 2008 to 2010. He is currently an Associate Professor in the State Key Laboratory of Information Engineering in Surveying, Mapping and Remote Sensing (LIESMARS), Wuhan University, Wuhan, Hubei, China. His research interests include hyperspectral data analysis, high-resolution image processing, and indexation of images at different resolutions.

Jocelyn Chanussot (Fellow, IEEE) received the M.Sc. degree in electrical engineering from the Grenoble Institute of Technology (Grenoble INP), Grenoble, France, in 1995 and the Ph.D. degree from Savoie University, Annecy, France, in 1998.

In 1999, he was with the Geography Imagery Perception Laboratory for the Delegation Generale de l'Armement (DGA—French National Defense Department). Since 1999, he has been with Grenoble INP, where he was an Assistant Professor from 1999 to 2005, an Associate Professor from 2005 to 2007, and is currently a Professor of Signal and Image Processing. He is currently conducting his research at the Grenoble Images Speech Signals and Automatics Laboratory (GIPSA-Lab), Grenoble, France. His research interests include image analysis, multicomponent image processing, nonlinear filtering, and data fusion in remote sensing.

Dr. Chanussot is the founding President of the IEEE Geoscience and Remote Sensing French chapter (2007–2010) which received the 2010 IEEE GRSS Chapter Excellence Award "for excellence as a Geoscience and Remote Sensing Society chapter demonstrated by exemplary activities during 2009." He was the recipient of the NORSIG 2006 Best Student Paper Award, the IEEE GRSS 2011 Symposium Best Paper Award, and the IEEE GRSS 2012 Transactions Prize Paper Award. He was a member of the IEEE Geoscience and Remote Sensing Society AdCom (2009–2010), in charge of membership development. He was the General Chair of the first IEEE GRSS Workshop on Hyperspectral Image and Signal Processing, Evolution in Remote sensing (WHISPERS). He was the Chair (2009–2011) and Cochair of the GRS Data Fusion Technical Committee (2005–2008). He was a member of the Machine Learning for Signal Processing Technical Committee of the IEEE Signal Processing Society (2006–2008) and the Program Chair of the IEEE International Workshop on Machine Learning for Signal Processing (2009). He was an Associate Editor for the IEEE Geoscience and Remote Sensing Letters (2005–2007) and for *Pattern Recognition* (2006–2008). Since 2007, he has been an Associate Editor for the IEEE Transactions on Geoscience and Remote Sensing. Since 2011, he has been the Editor-in-Chief of the IEEE Journal of Selected Topics in Applied Earth Observations and Remote Sensing.